DAMAGE EVALUATION IN DOLOMITIC LIMESTONE USING NONLINEAR ULTRASONIC HIGHER HARMONIC GENERATION

BY

RUOLEI WANG

THESIS

Submitted in partial fulfillment of the requirements
for the degree of Master of Science in Systems and Entrepreneurial Engineering
in the Graduate College of the
University of Illinois Urbana-Champaign, 2022

Urbana, Illinois

Adviser:

Professor Henrique M. Reis

ABSTRACT

Dolomitic limestone specimens were increasingly damaged by heat treating them to 100 °C, 200 °C, 300 °C, 400 °C, 500 °C, 600 °C and 700 °C. Along with an undamaged specimen, all specimens were nondestructively tested using nonlinear higher harmonic generation method. The flexural strengths of the specimen were also obtained through four-point bending tests to validate the strength reduction caused by accumulation of microcracks through high temperature treatment. Results from higher harmonic generation method correlated relatively well with the corresponding strength reduction in each specimen ($R^2 = 0.91$ for 3rd order amplitude ratio and $R^2 = 0.84$ for 5th order amplitude ratio), which matches with some of the finding conducted by previous studies. However, the results were also greatly influenced by the frequency of the sending waves. The application of this method should be introduced with other well-established methods such as noncollinear wave mixing to increase its reliability.

ACKNOWLEDGEMENTS

There's nothing easy about this journey, particularly if you choose to start it at an uncertain time. However, I'm very grateful that I managed to accomplish this at the time of COVID because it educates me to be patient, it toughens my mind, it confirms my willingness to dedicate myself to the world of scientific research. To this, I would like to thank these three years I spend in Champaign. What a time!

I can't say how grateful I'm to join NDT lab at the time when I was most confused. Professor Reis let me join the lab and I think it is one of the most fruitful decisions I've ever done. Professor Reis has given me support through several ways: the academic support, the lengthy yet delightful life wisdom, the patient to a research novice, and several free meals and coffees. To this, I would like to thank the eternal Godfather of TB400, Professor Henrique M. Reis.

A good friend is like a teacher to self, and that is exactly what Josh is to me. As the senior member of the lab, I've learned so much from him and I hope that I can be as good as he is in the near future. Plus, we had so many good times at lab. To this, I would like to thank my friend and my only lab mate, hopefully not for anytime longer, Joshua Love.

There are so many people who support me during my time pursuing master's degree. My dear friends, Benny, Zihao, Chi, Annie, Robert and so much more people have given me good advice and enjoyable times at the hard time of COVID and it means a lot to me. Thank you all.

My family has been, unquestionably, the biggest support for me. Although I cannot be with them to celebrate and enjoy this honor with me at the same place, there's no way I can achieve this accomplishment without their love. I love you all.

At last, I want to dedicate this to my grandfather, Guozhen. In some way, he is my first teacher to the world of science. As a teacher himself, his dedication on the education of every student he taught has been one of the most important inspirations for me. I cannot think of a better way to honor him other than my first academic accomplishment.

To my grandfather, Guozhen

献给我的姥爷，王国振

TABLE OF CONTENTS

LIST OF FIGURES

CHAPTER 1: INTRODUCTION

1.1 Problem Statement

Limestone is one of the most widely used building materials, comprising 10% and more of all sedimentary rock in the world. It is composed mostly of minerals calcite and aragonite, which are different crystal forms of calcium carbonate ($CaCO_3$) [1-3]. First identified from limestone by Baltazar Hacquet, Dolomite [$CaMg(CO_3)_2$] forms as a result of exposure of calcium carbonate to magnesium ions. Dolomitic limestone, as shown in Figure 1.1, refers to limestone that contain significant amounts of dolomite, usually from 10% to 50% [1,4].

Figure 1.1: Dolomitic Limestone piece [40], reproduced from Wikimedia.

Throughout the history, stone are used in buildings for constructional purposes like the Tower of London, the Great Wall of China and The Great Pyramid in Giza. From 1800s, limestone gradually lost its edge to steel frame as the better choice for load bearing material, but remained great appearance for non-load bearing, decorative usage [3,5-7]. Since the 1960s, standardization for limestone cladding has been pushed throughout the globe with some of the most common applications like the façades of architectural application and stone-faced composite planes [8].

A study conducted by Chin determined that 40% of strength reduction failures are due to exposure to weather, e.g., temperature variations. Additionally, 45% of failures were due to failure of the

connection between the cladding and the building and 15% of failures were due to water leakage [8]. While numerous regulation and codes are set around the problem of linkage failure and water leakage, limited numbers of regulation cover the importance of reduction in strength due to temperature variation [9-12]. In a recent study on cladding panels, Schoeuenberg [13] reviewed 100 years' worth of research into different stones, especially focusing on the causes of deterioration of stone paneling. One of the largest factors contributing to the failure of stone failure is thermal hysteresis combined with relative high moisture contents [18].

1.2 Research Objective

In some previous studies [7,14-17], non-linear properties of limestone have been studied. In three of the previous studies [7, 14-16], several heat-treated specimens at various temperature are investigated using non-linear wave mixing technique. In these studies, a receiving transducer was incidentally mounted on the dolomitic limestone specimen surface to detect the generated shear horizontal nonlinear wave from sending dilatational transducers. The goal is to determine if the flexural strengths of heat-treated limestone specimens are correlated with one of the physical characteristics of the limestone, which in these cases is non-linear wave generation parameter, i.e., β value [7]. In Shah's study, non-linearity of concrete in view of the second and third-order or higher frequency components occurrence in addition to the fundamental one is reviewed [17]. Two dilatational transducers are vertically mounted and fastened at the standing surface of a cube concrete specimen, with one sending the signal and one receiving. While the specimen is compressed, the wave signal is collected and the ratio between the amplitude at main frequencies and the amplitude at higher harmonic frequencies are used to describe the level of damage.

This study aims to find the correlation between the amplitude ratio of main frequency to higher harmonic frequencies and physical performance of heat-treated Dolomitic limestone specimen, specifically regarding towards flexural strength reduction. In this study, one dilatational wave is generated by a dilatational transducer and received by another one, both incidentally mounted against two parallelly surfaces, which is shown in Figure 5.1. Please note that due to the geometry of the specimens and transducer, the mounting position is not always at a pre-determined location

but is chosen to have no visual defects and large enough space for transducer to be attached on. After the signal was captured and processed, amplitude ratio trend between main frequency and higher harmonics will be compared to results obtained in previous studies.

1.3 Thesis Overview

Chapter 2 provides a literature review of topics relevant to this study. Discrimination of Limestone and Dolomite and their application history, an overview of weather factor to the failure of limestone, calcination of limestone, review on non-destructive testing investigating non-linear higher harmonic generation and existed research on evaluation of damage in limestone will be presented in that order.

Chapter 3 provides explanation and mathematic review for higher harmonic generation used in this study.

Chapter 4 describes how the experiment was prepared.

Chapter 5 describes the experimental setup and the data collection and analysis process.

Chapter 6 presents the results of the experiment including amplitude ratios between main frequency and higher harmonics and their relationship to the strength of the specimens. The resulting trends will be compared with previous four studies conducted by McGovern and Reis in 2017 [16], Love and Reis in 2019 [7] and Shah and Ribakov in 2009 [17] to determine if Higher Harmonic generation has correlation to the level of damage of the specimen.

Chapter 7 present conclusions to this study and some suggestions on application of this study.

Appendix describes the switching technique to obtain attenuation coefficients of the material.

CHAPTER 2: LITERATURE REVIEW

2.1 Discrimination of Limestone and Dolomite and their application history

Limestone is one of the most widely used building material throughout time and across the globe. Thanks to its wide availability, appealing appearance and relative strong physical property, it was used as structural and decorative material in various buildings [1,2]. For instance, the Tower in London in Figure 2.1 is building around the White Tower, which is constructed by limestones as it appears in yellow and gray color. The Tower of London was served as one of the most iconic fortress and getaway to the capital of Norman Empire [20], indicating the reliability and appealing of limestone as a building material to the Royal power.

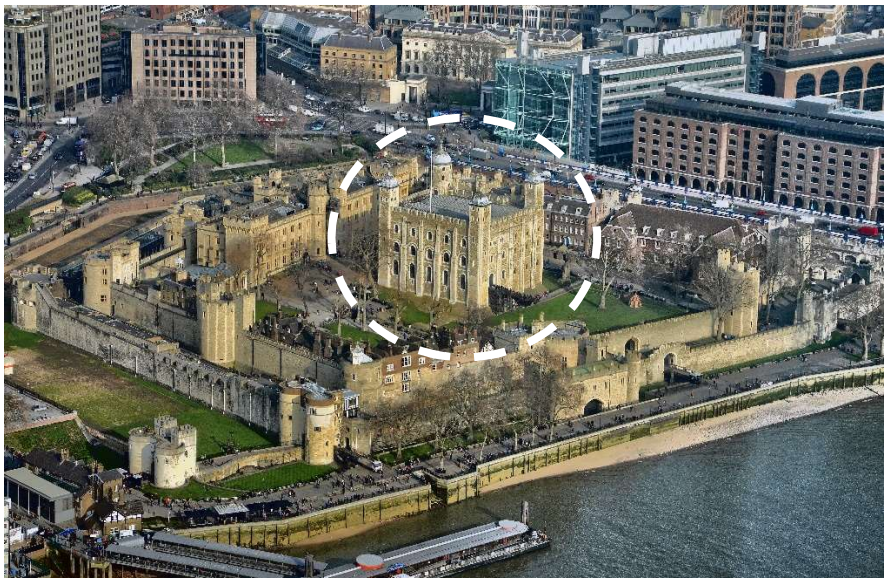

Figure 2.1: The Tower of London, with The White Tower circled at the middle [19], reproduced from Wikimedia.

Dolomite was first distinguished by Baltazar Hacquet in 1778 [4] from Limestone as an independent substance in geology. However, the term Dolomitic Limestone was used for limestone that contains significant amount of dolomite. In terms of application, Dolomitic Limestone shares very similar working scenarios as regular limestones, especially in construction.

Since the 1800s, the First Industrial Revolution made steel a more reachable material and in constructional field it quickly replaced the place of stone as the load bearing structural material

[5,6]. But due to its great appearance and wide availability, stone is still used as non-loading decorative material, mostly in forms of standardized cladding and panels. Mostly anchored to masonry, concrete and steel, some panels are used as part of the load bearing façades and others are used purely for decorative purposes. Figure 4.2 gives some applications for stone panels in different time eras.

Figure 2.2: Photos of Ohio Statehouse built in 1861 (left) [42] and Romanian People's Palace built in 1997 (right) [43], reproduced from Wikimedia.

Apart from architectural applications, limestone and dolomite have other significant application. Limestone is used as an aggregate for cement concrete and asphalt concrete [21, 22]. Dolomite rock can act as an oil and natural gas reservoir and dolomite is also used in the manufacture of refractory materials. It is worth noting that many other stones materials are also used for architectural, structural and engineering applications including marble, granite and quartzite [7]. The application of this study may also be repeated on these stone materials and is expected to exhibit similar results.

2.2 An overview of weather factor to the failure of limestone

When used in engineering applications, stone cladding is the major form in use, typically a 3/8 in (10 mm) aluminum honeycomb core, sided by a 1/16 inch (1.5 mm) layer of stone (facing the outside) and by a thin light-weight reinforced polymeric composite layer such as a reinforced glass fiber composite panel [7,8]. These panels are exposed to the weather and may experience damages like warp, dish or bow that reduce the integrity of the stone cladding and may even cause danger to people nearby.

Despite of the potential danger of failing stone cladding, it is hard to set up standards to control the level of damage caused by weather. This is because the weathering of stone generally occurs with a variety of mechanisms working together, or at least depending on current research [18]. Acid dissolution, frost action, salt crystallization, and anisotropic thermal expansion have all been identified as mechanisms that can damage stone and induce deformation [18, 24-26]. In previous studies and for the specimens used in this study, Anisotropic thermal expansion is applied to induce controlled damage. Through such deformation, induced stresses will cause microcracks forms along the grain boundaries and create diffuse damage within the material [7]. With water presented in pores formed in microcracks, thermal damage will be worsened by the pressure applied onto the anomalies. It is worth mentioning that although such mechanisms will be needed in preparation for the specimen, it might also cause some damage that is not desired by this study like uneven surface or destructive cracks. This may cause some deviation to expectation as will discussed in Chapter 6.

A study conducted by Chin [8] determined that 40% of strength reduction failures are due to exposure to weather, e.g., temperature variations. Additionally, 45% of failures were due to failure of the connection between the cladding and the building and 15% of failures were due to water leakage [8]. While numerous regulation and codes are set around the problem of linkage failure and water leakage, limited numbers of regulation cover the importance of reduction in strength due to temperature variation [9-12]. In a recent study on cladding panels, Schoeuenberg [13] reviewed 100 years' worth of research into different stones, especially focusing on the causes of deterioration of stone paneling. One of the largest factors contributing to the failure of stone failure is thermal hysteresis combined with moisture [18].

2.3 Calcination of Limestone

The specimens use in this study, dolomitic limestone, will undergo a chemical reaction which decomposed as following [27]:

$$CaCO_3 \cdot MgCO_3 + Heat_{(1)} \leftrightarrow CaCO_3 \cdot MgO + CO_2 \uparrow \quad (1)$$

$$CaCO_3 + MgO + Heat_{(1+2)} \leftrightarrow CaO \cdot MgO + CO_2 \uparrow \quad (2)$$

In some cases, this reaction will happen in one stage depending on the specific properties of limestone in question [27]:

$$CaCO_3 \cdot MgCO_3 + Heat_{(1+2)} \leftrightarrow CaO \cdot MgO + 2CO_2 \uparrow \quad (3)$$

And when given access to moist environment, Calcium Oxide (CaO) will quickly turn in to portlandite ($Ca(OH)_2$) [29]:

$$CaO + H_2O \leftrightarrow Ca(OH)_2 + Heat \quad (4)$$

Such process is referred as "Calcination of Limestone". This effect will initiate from 510 °C to 750 °C, with specific temperature being determined by crystal structure and of the stone in question [27,28]. This is an irreversible alternation to the property of the stone, which will be shown in Chapter 6 and 7 when data is presented.

The reason Calcination is important to this study is that two of the prepared specimens used in this study has experienced and are only able to experience significant effect of calcination as they are heat treated around the initiating temperature. Detail of the specimen plus its preparation will be provided in Chapter 4. One thing to be notice that in engineering applications, seldom practices' exerting temperatures will be able to induce calcination reaction and so does long time exposure to high exterior temperature for extensive periods of time will affect limestone material. Whereas in case of fire, temperature will reach high enough to cause calcination. It is reasonable, and being developed by previous studies [7, 14-16], for nondestructive testing to evaluate the level of damage and safety issues of a building or infrastructure following a fire. Chapter 7 will cover how to evaluate damage from fire.

2.4 Review on nonlinear higher harmonic generation

The reason why non-linear response is chosen for this study comes from numerous reports that decrease in pulse amplitude (attenuation) and shifts in peak frequency are more sensitive and reliable to characterize distributed damage in the form of diffuse flaw populations, i.e., microcracking than traditional linear response analysis [30, 31].

For ultrasonic test, linear analysis typically consists in obtaining the longitudinal and shear velocities and their corresponding attenuations. Generally, linear ultrasonic analysis is valid as long as the wavelength of the sending signal is smaller than the width of the defects. However, in case of distributed micro flaw populations through damage like fatigue, heat treatment or chemical attack, linear analysis is not the best choice. On the other hand, non-linear response analysis often uses harmonic generation [32]. A signal with large enough amplitude to be detected on the other side will be launched from one side of the material and received from the other side. Once signal is collected, the detected waveform often consists of not just the component from the sending frequency, but also at frequencies that are the integer multiple of the sending frequency. This is result from the non-linear interaction between ultrasonic wave and the material it traveled through [33]. Typically, the magnitude of non-linear interaction will increase as the damage increase.

As a result of the sensitivity to all kinds of damage, non-linear method is more effective than its linear counterparts in the area of micro-damage evaluation. Some of the recent research has been conducted around this area. Selleck et al. used ultrasonic longitudinal pulses to evaluate damage on concrete due to freeze–thaw cycles and salt scaling [30]. They have studied changes in pulse velocity, attenuation and the peak frequency. Suaris et al. used ultrasonic pulse attenuation to determine the damage growth of the concrete [31]. Shah et al. used longitudinal pulse to evaluate damage on concrete under different loading situation and track the higher harmonic amplitude response [17].

2.5 Existing research on evaluation of damage in dimension limestone

Limestone, specifically the limestone specimen that used in this study, has a brick-and-mortar type microstructure which exhibits nonlinear mesoscopic elastic behavior [34,35]. In limestone, the bricks (i.e., grains, crystals, impurities) share same elastic behavior as they interface with each other across an elastic system. The mortar is a system of asperities that holds the bricks together at grain/crystal boundaries [7], and because most of the deformation happens in mortar, the mortar is responsible for most nonlinear response in limestone. Another reason for the nonlinear behavior

comes from weathering. Freeze-thaw cycles, acid dissolution, frost action and salt crystallization will cause micro defects appears in large population all over the material [24]. With this kind of defects, limestone becomes more sensitive to microcrack coalescence and thus increase the possibility of nonlinear behavior presence in the material [17]. In order to examine the damage on materials using higher harmonic, several studies have been conducted and nonlinear behavior has been exhibited [36-39]. Also, there are several studies that try to evaluate the damage using different methods like nonlinear wave mixing [7,14-16].

One of the studies that utilized higher harmonic method is conducted by Shah and Ribakov in 2009 [17]. Several cubed concrete specimens with different water to cement ratio are put under a compressing machine with 2 transducers attached to countering faces, one sending the signal and the other receiving it. Frequency signals were collected at different compressing level under the ultimate strength. This study measures two set of ratios: Amplitude (A_2) at second harmonic frequency (f_2) vs. the square of Amplitude (A_1^2) at sending frequency (f_1); Amplitude (A_3) at third harmonic frequency (f_3) vs. the cube of Amplitude (A_1^3) at sending frequency (f_1). It has shown that with a high enough amplitude sending signal, the ratio of A_2/A_1^2 and A_3/A_1^3 will increase as the damage increase, and such effect will exaggerate when the damage reaching closer to the ultimate strength.

Another study using higher harmonic method is to investigate fatigue damage at nickel-based super alloy [34]. Kim et al. used 2 transducers attached to countering faces, one sending signal and one receiving. The specimen is attached to fatigue loading setup where 0.5Hz and 1Hz cyclic loadings are used. Through collected data, the normalized nonlinear wave generation parameter (β/β_0) is obtained through comparing amplitude at main frequency and different harmonic frequencies. This is a more generalized and wide-used parameter to compare as shown in many other studies. After that, β/β_0 is compared to the fatigue life of the specimen and a positive correlated relationship is established, meaning the higher harmonic behavior can help determine distributed microdamage and remaining useful life of the specimens.

There are also studies that are conducted on the same specimens used in this study to evaluate nonlinear behavior but using a different method [7,14-16]. The method in application is called non-collinear wave mixing, and it utilizes two transducers to send signals which intervent with each other instead of superposition like in linear application. The resulting signal will help to determine nonlinear wave generation parameter (β) as an indicator to the level of damage upon the material. The McGovern and Reis study [15] explored two experimental setups for non-collinear wave mixing. One of the setups sends waves from the top surface of a specimen at an angle and the interacting wave is received from the bottom of the specimen. The other setup sends the wave in the same wave, but the receiver is mounted close to its perpendicular front surface. A longitudinal transducer will collect data from that surface. Noting that although the interacting wave under the wave mixing theories is a shear wave which do not transmit near the surface, some of the energy in shear wave will be converted into longitudinal wave because of the granite, i.e., the dispersive nature of the material. In their 2015 study, McGovern and Reis [14] study utilized critically refracted subsurface waves. Two longitudinal transducers to send signal are mounted on polymathic shear wedges then to the surface of the specimen. Another longitudinal transducer is mounted incidentally to the surface to detect signal that was mixed. One of the advantages of this setup is that it can be done with just one side accessible. In 2019, Love, McGovern and Reis used shear transducer instead of longitudinal as the receiving transducer and investigate how is the placement of the transducer affect the detection of the resultant wave.

These studies provide reasonable expectations for the result and trustable case for the effectiveness of higher harmonic application. With the results and methodologies provided in the previous experiment, the result of this study should be reliable as long as the damage evaluation trends agree.

CHAPTER 3: HIGHER HARMONIC GENERATION

3.1 Higher harmonic generation

As discussed in previous chapters, weathering over extensive interval of time will cause microcracks and distributed damage along the material. As damage progress with time and weather conditions, microdamage coalesce into larger crack and may cause failure inside the material. This effect will also cause more nonlinear wave behavior as the material becomes less isotropic and the waves can further interact with the larger microcracks more. More and more energy will be converted to higher harmonics as damage increases.

The non-linear wave equation used in this study for describing the observed behavior is well discussed in reference [17], and presented below:

$$\frac{\partial^2 P_\Psi}{\partial t^2} = c_\Psi^2 \left[1 - \beta_\Psi \left(\frac{\partial P_\Psi}{\partial d_1}\right)\right] \frac{\partial^2 P_\Psi}{\partial x_1^2} \tag{5}$$

Here P_Ψ is the displacement of the waveform with respect to time; c_Ψ is the linear wave velocity; β_Ψ is the Acoustic nonlinearity parameter; x_1 is the wave propagation distance. For the case in this study, P_Ψ is expanded as follows:

$$P_\Psi = P_\Psi^{(1)} + P_\Psi^{(2)} + H.O.T \tag{6}$$

where $P_\Psi^{(1)}$ is the linear differential solution describing the wave

$$\frac{\partial^2 P_\Psi^{(1)}}{\partial t^2} = c_\Psi^2 \frac{\partial^2 P_\Psi^{(1)}}{\partial x_1^2} \tag{7}$$

At $a_1 = 0$, the solution of Eq. (7) will be

$$P_\Psi^{(1)} = A_1 \cos\left(k_\Psi x_1 - \omega t\right) \tag{8}$$

where $P_{\Psi 1} = \left|Max\left(P_\Psi^{(1)}\right)\right|$, k_Ψ is the mode wave number.

Substituting Eq.(8) into Eq.(5),

$$\frac{\partial^2 P_\Psi^{(2)}}{\partial t^2} = c_\Psi^2 \frac{\partial^2 P_\Psi^{(2)}}{\partial x_1^2} - \frac{1}{2} c_\Psi^2 \beta_\Psi k_\Psi^3 (A_1)^2 \sin^2(k_\Psi d_1 - \omega t) = c_\Psi^2 \frac{\partial^2 P_\Psi^{(2)}}{\partial x_1^2} - S \tag{9}$$

Here S is the nonlinear term that represent the second harmonic sinusoid. A general solution to Eq.(9) is as follows [38]:

$$P_{\Psi}^{(2)} = f(x_1)\sin^2(k_{\Psi}x_1 - \omega t) + g(x_1)\cos^2(k_{\Psi}x_1 - \omega t) \tag{10}$$

Substituting Eq.(10) into Eq.(9),

$$\left(4k_{\Psi}\frac{df}{dx_1} + \frac{d^2g}{dx_1^2}\right)\cos^2(k_{\Psi}x_1 - \omega t) - \left(4k_{\Psi}\frac{dg}{dx_1} + \frac{d^2}{dx_1^2}\right)\sin^2(k_{\Psi}x_1 - \omega t) = \frac{1}{2}\beta_{\Psi}k_{\Psi}^3(A_1)^2\sin^2(k_{\Psi}x_1 - \omega t) \tag{11}$$

Assuming that

$$4k_{\Psi}\frac{df}{dx_1} + \frac{d^2g}{dx_1^2} = 0 \tag{12}$$

$$4k_{\Psi}\frac{dg}{dx_1} + \frac{d^2}{dx_1^2} = -\frac{1}{2}\beta_{\Psi}k_{\Psi}^3(A_1)^2 \tag{13}$$

$$\frac{df}{dx_1} = \frac{d^2g}{dx_1^2} = 0 \tag{14}$$

This means that Eq.(12) and (13) is hold consistently.

Now, substituting Eq.(4) and (5) into Eq.(2),

$$P_{\Psi} = A_1\cos(k_{\Psi}x_1 - \omega t) - \frac{1}{8}\beta_{\Psi}k_{\Psi}^2(A_2)^2x_1\sin^2(k_{\Psi}x_1 - \omega t) + \cdots \tag{15}$$

This shows that the signal amplitude $P_{\Psi 2} = \frac{1}{8}\beta_{\Psi}k_{\Psi}^2(P_{\Psi 1})^2x_1$. Therefore, it can be shown that there should be a linear relationship between the amplitude of the second harmonic and square of the amplitude of the main frequency. This linear relationship, all referred later as the amplitude ratio, can also be found in $P_{\Psi 3}/P_{\Psi 1}^3$. To be more specific,

$$\frac{A_2}{A_1^2} = \frac{\beta_2}{4}k^2x_1 \tag{16}$$

$$\frac{A_3}{A_1^3} = \frac{\beta_3}{8}k^3x_1 \tag{17}$$

From this, it is reasonable to expect that for higher harmonics, n-th harmonic frequencies' amplitude will be in a linear relationship with the n-th power of the main frequency amplitude:

$$\frac{A_n}{A_1^n} = C = \frac{\beta_n}{2^n} k^n x_1 \tag{18}$$

3.2 Absence of even harmonic

In this study, it is to be expected that harmonic behavior happens at consecutive harmonic frequency, namely at 2,3,4,… times of the main frequency, i.e., there will be a spike of amplitude in frequency domain signal. However, this is not true for this study. Several reasons are considered.

Typically, one of the possible reasons comes from the wave modes used and material microstructure. In Srivastava's study in 2009 [46] of antisymmetric and symmetric plate wave as well as surface wave, it was found that antisymmetric modes can only exist at odd harmonics $(3\omega, 5\omega, 7\omega, \dots)$, whereas symmetric modes can exist at both odd and even $(2\omega, 4\omega, 6\omega)$ harmonics. In this study, only a longitudinal wave was sent.

A more likely explanation is the abnormally high third harmonic in the presence of damage at grain boundaries [43,44]. The main reason behind that is unusually high 4^{th} order non-linearity of defective materials permitting the third harmonic to be generated by direct four-wave process: $\omega + \omega + \omega \rightarrow 3\omega$ instead of the typically generated two subsequent three-wave interactions: $\omega + \omega \rightarrow 2\omega$ and $2\omega + \omega \rightarrow 3\omega$ [43].

Other possible explanations may include potential guided wave effects that may lead to the absence of harmonic behavior [45]; higher harmonic frequencies are far out of the range of half-amplitude bandwidth of the transducer in use, causing lower readout at high end of the frequency. However, since this study is only focus on the amplitude ratio, reasonable conclusion can still be conducted from detected harmonics response.

3.3 Attenuation

The ultrasonic attenuation is one of the fundamental acoustic parameters of a material. It is a macroscopic parameter containing information about a material's microstructure such as grain structure, inhomogeneity and dislocation. In order to obtain the attenuation, a switching technique is applied in this study [49]. The detail on the switching technique for attenuation coefficient measurement is provided in Appendix B. Amplitude attenuation can be expressed using following equation:

$$A_{1r} = A_1 \exp(-\alpha d) \tag{19}$$

Here, A_{1r} is amplitude of the signal received, A_1 is the adjusted amplitude of the signal expecting no attenuation, α is the attenuation coefficient and d is the distance traveled.

Therefore, the n-th order amplitude ratio can be expressed as:

$$\frac{A_n}{A_1^n} = \frac{A_{nr}}{A_{1r}^n} \exp(\alpha_n d - n\alpha_1 d) \tag{20}$$

For this study, second, third and fifth order amplitude ratio will be used.

CHAPTER 4: EXPERIMENT PREPERATION

4.1 Specimen Preparation

This study uses the same samples as used in McGovern and Reis, 2015 and in Love, McGovern and Reis, 2019 [7,14]. Eight Samples of Illinois dolomitic limestone salvaged from windowsills were cut into blocks with nominal dimensions of 185 mm x 155 mm x 65 mm. The heating process used by discussed by Scherer and his associates [47, 48] was used to induce controlled artificial damage. Seven specimens are individually heated to 100 °C, 200 °C, 300 °C, 400 °C, 500 °C, 600 °C and 700 °C at rate of 150 °C per hour from room temperature of approximately 25 °C. The samples were then kept at that temperature for 90 minutes instead of 60 minutes used by Scherer and his associates [47,48] to ensure uniform distribution of stress and damage, as the specimens in this experiment were larger than those used by discussed by Scherer and his associates. After heating, the oven was turned off and the samples were left inside to cool overnight. Then, the specimens were cut into smaller cylinders in dimension of 185mm x 65mm x 55mm for the convenience of measurement as shown in Figure 4.4. Note that one of the specimens was cut in shape as in Figure 4.4 (right) for other purpose but this does not affect the result of this test.

4.2 Linear Characterization

The linear acoustic properties of the test specimens, i.e., their dilatational and shear velocities and the corresponding attenuations were obtained and reported in [14]. Figure 4.1 shows the dilatation and shear velocities and corresponding attenuations as a function of damage. The data and the figure were reproduced with permission from McGovern and Reis [14]. For additional discussion on specimen preparation and their linear characterization, please refereed to McGovern and Reis [14]. Figure 4.2 shows the specific attenuation coefficient in 300 kHz and 600 kHz for 25 °C, 100 °C, 200 °C, 300 °C and 400 °C specimens. Note that for specimen that is heated to 500 °C and above, signal component above 500 kHz is low enough to ignore.

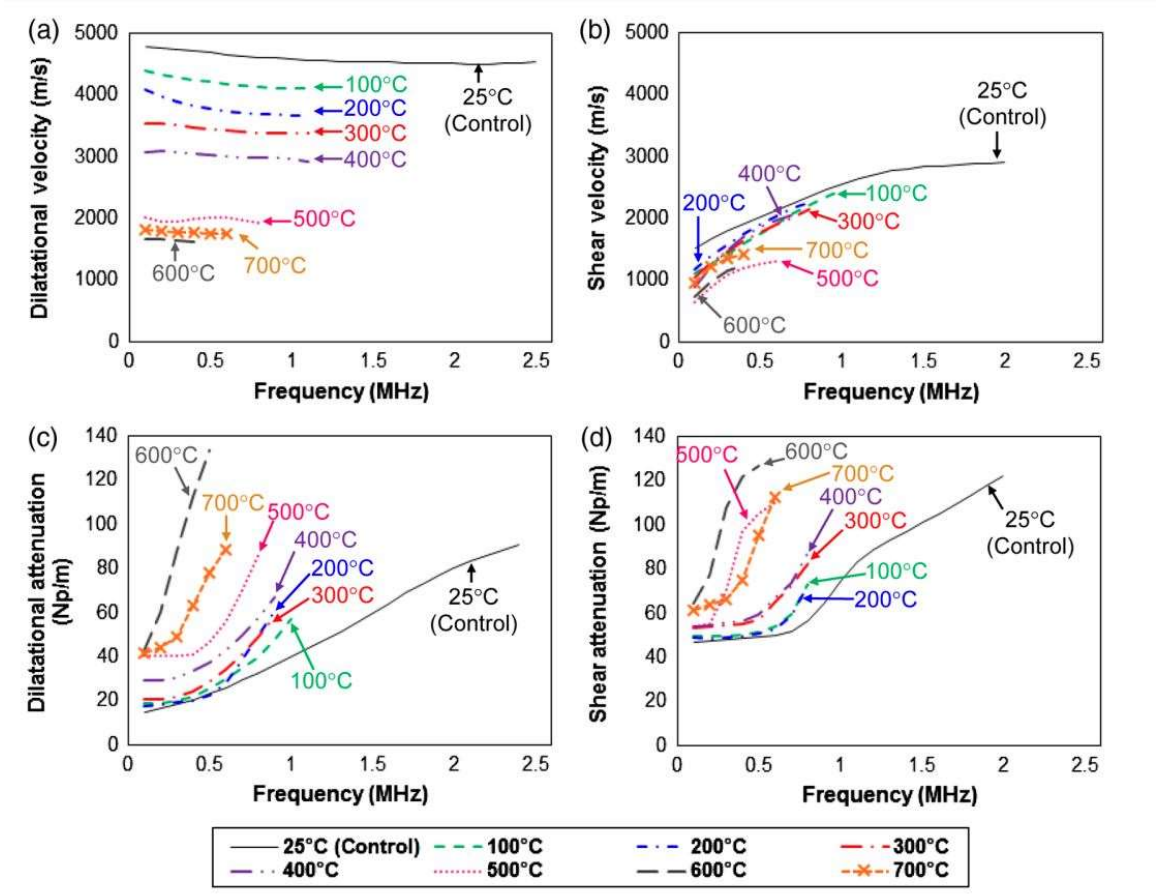

Figure 4.1: Phase velocities and corresponding attenuations: (up left) dilatational and (up right) shear phase velocities (m/s) as a function of frequency for the limestone specimens heated to various temperatures: (low left) corresponding dilatational and (low right) shear attenuations (Np/m) as a function of frequency for the limestone specimens heated to various temperatures. Figure reproduced from McGovern and Reis [14].

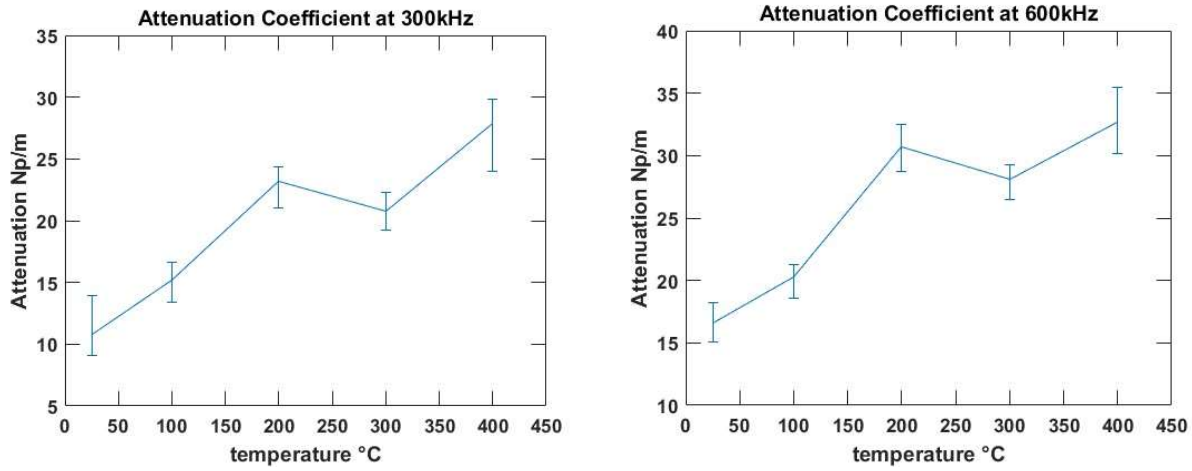

Figure 4.2: Attenuation coefficient for different temperature specimen at 300 kHz (left) and 600 kHz (right). Current attenuation measurements are consistent with those observed in Figure 4.1.

4.3 Flexural Strength

To determine the flexural strength in each specimen, five beam samples were cut from remaining part of each specimen with nominal dimensions of 180mm x 55mm x 15mm. The dimensions of the specimen were set to satisfy the slenderness assumption of beam theory ($h \leq 10L$). Before any test was conducted, all samples were conditioned in an oven at 60 °C for 15 hours to eliminate any water residual. After 13, 14 and 15 hours in the oven, the samples were weighed to ensure constant weight that implies the samples were completely dry. Then the prepared samples were loaded under a four-point bending setup with a supporting span of 160 mm and loading span of 40 mm. The loading rate of the setup is set at 0.05mm/min. Load and displacement measurements were taken until the specimens fractured. The testing was conducted in accordance with ASTM standard (ASTM C 880-06, 2007). Specimen width did not meet the standard, as dimensions were limited by original specimen geometry. Reduction in strength was measured with respect to the average strength of the control specimen in order to measure percentage reduction in strength. Figure 4.3 shows the average percent reduction in strength to undamaged specimen. The data and the figure were reproduced with permission from McGovern and Reis [14]. For additional discussion on flexure strength over the specimen used in this study, please refereed to McGovern and Reis [14].

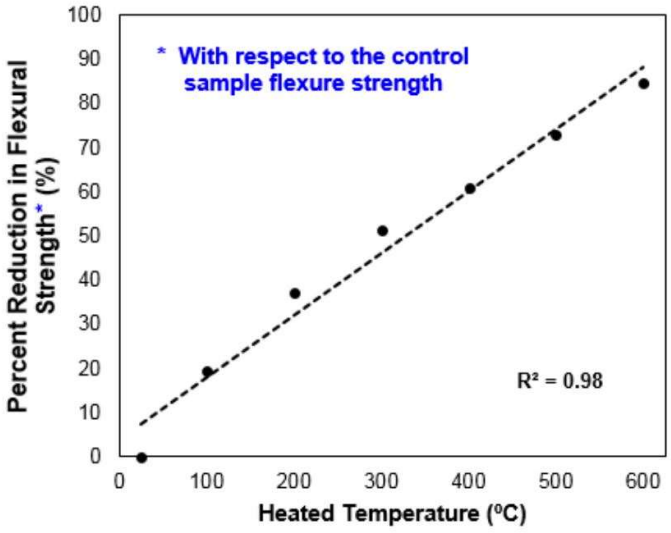

Figure 4.3: Mean percent reduction in flexural strength (percentage) of heated samples with respect to the mean flexural strength of the control sample. The flexural strength for each specimen was averaged from five samples. Figure reproduced from McGovern and Reis [14].

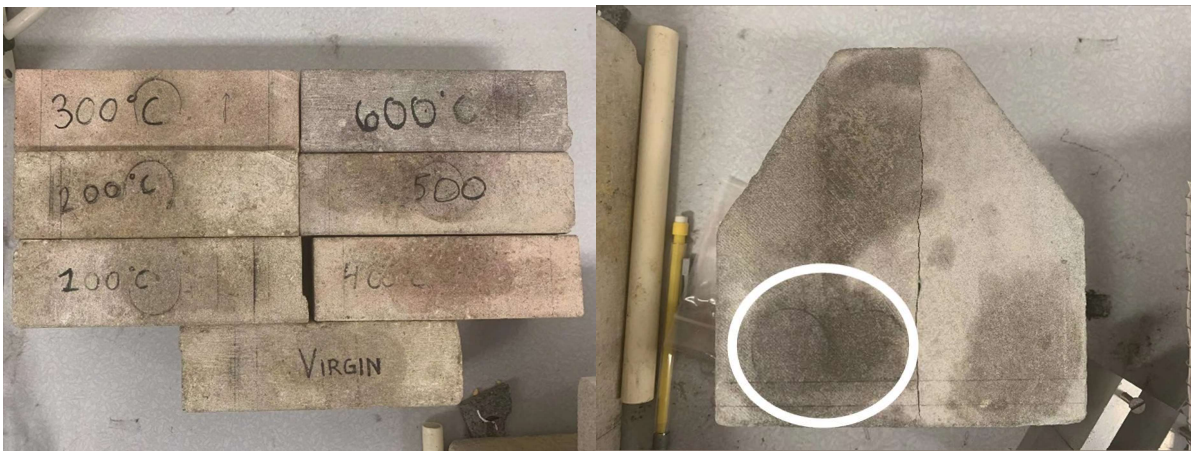

Figure 4.4: Photos of tested specimen in this study. Temperature of heat treatment for each specimen has been labeled (left), with virgin specimen not being heat treated. 700 °C Specimen (right) is in a different shape that is used in [7,14] and appears more white-colored than other specimens due to calcination. Dark spots (circled spot) come from the residuals of high vacuum grease used to affix transducers to the specimen.

CHAPTER 5: EXPERIMENT SETUP AND DATA ACQUISITION.

Two longitudinal transducers are incidentally mounted and to the specimen and aligned as shown in Figure 5.1. One transducer will send a wave signal and one will receive. The mounting position are chosen to be relatively away from the corner position in order to eliminate guided wave effect at the best. For this study, two sets of transducers are used to send 100 kHz waves (Panametrics V1011, center frequency 100 kHz) and 300 kHz waves (Panametrics V101, center frequency 500 kHz).

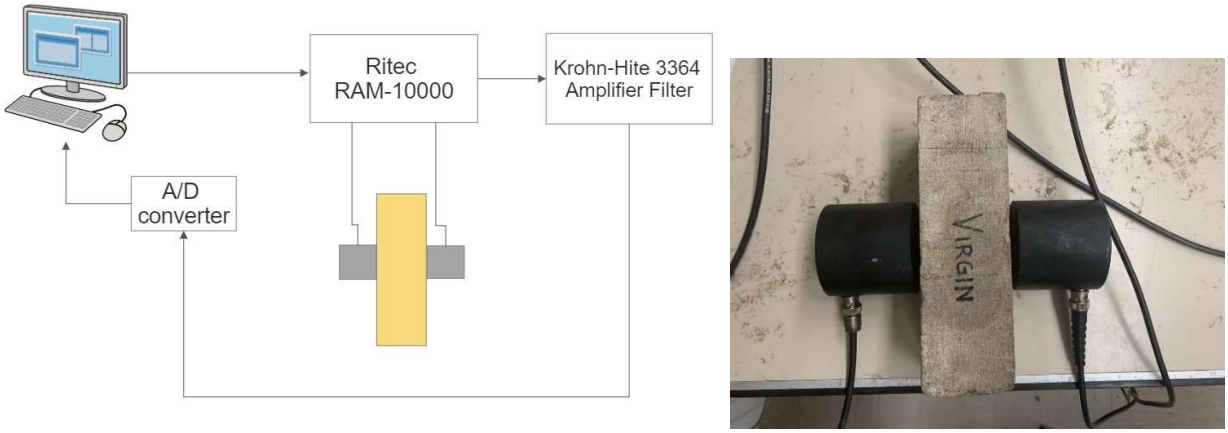

Figure 5.1: A schematic diagram of the experiment setup (left) with the configuration of transducer circled in red square. A photo of the transducer configuration (right) is shown.

A schematic diagram for the experimental setup is shown in Figure 5.1. Here, a RITEC advance measurement system RAM-10000 is used to generate 5 cycles of sinusoidal tonebursts into the sending transducer and receive the signal. The signal is then sent to a Krohn-Hite 3384 Amplifier/Filter, then digitized with an analogue to digital converter STR 825 and sent to a computer for data storage and analysis. Please note that due to the limitation of the used equipment, all receiving signals must be amplified to a peak amplitude that is lower than 1 Amp. 100 kHz signals were filtered through a high-pass filter of 50 kHz and 300 kHz signal were filtered through a high-pass filter of 200 kHz.

Once the data is collected, the time domain signal data will be converted to frequency domain signals using Fast Fourier Transform (FFT). Figure 5.2 shows a time domain signal and frequency

domain signal graph in 100 °C specimen with 100 kHz. All the peak amplitudes will be picked up through data analysis process.

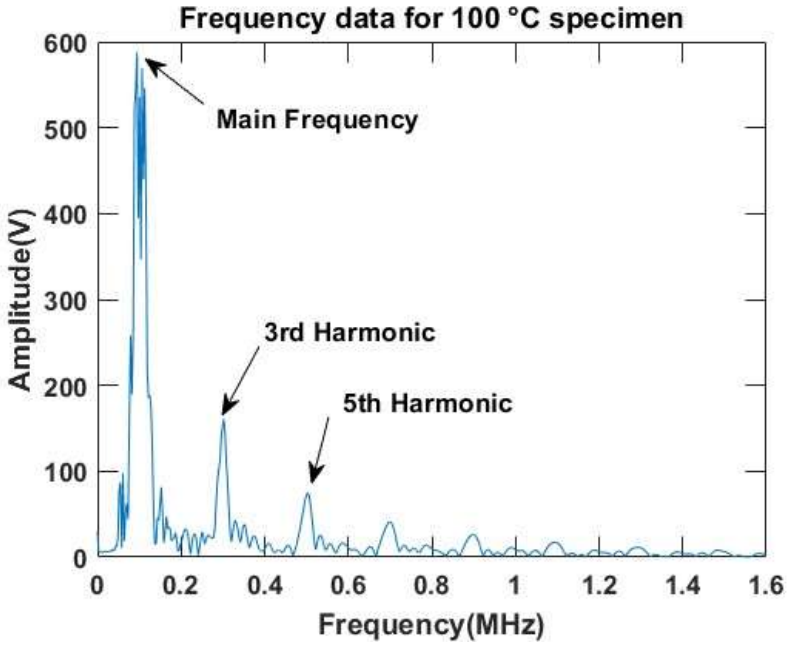

Figure 5.2: Frequency domain signal for 100 °C specimen showing amplitude vs. frequency. Amplitudes at main frequency (100 kHz) and harmonic frequencies (300 kHz and 500 kHz) are collected to determine the amplitude ratio. Note that even harmonic is not excited in this case.

CHAPTER 6: EXPERIMENTAL RESULTS

As showed in Figure 6.1, the third order and fifth order amplitude ratio of the specimens used in this study at 100 kHz shows an increasing trend from the lower temperature to higher temperature. This trend fit with the flexural strength to normalized wave generation parameter relationship found in previous studies [7,14], according to Figure 6.2. Note that the increasing trends are not necessarily linear or exponential or logarithmic from 200 °C to 600 °C, meaning that different order of amplitude ratio may corresponding to different properties of the material.

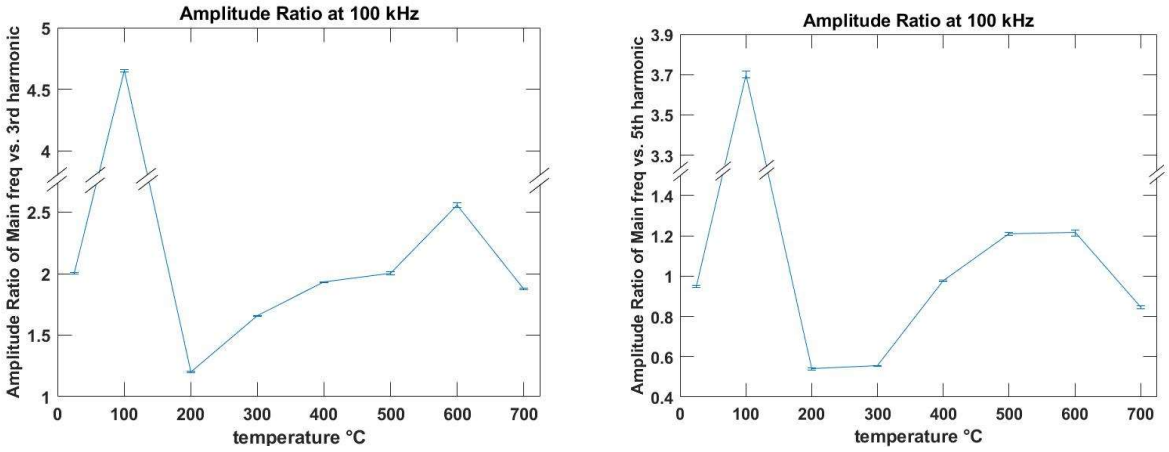

Figure 6.1: 3rd (right) and 5th (left) order Amplitude Ratio at 100 kHz for different specimens.

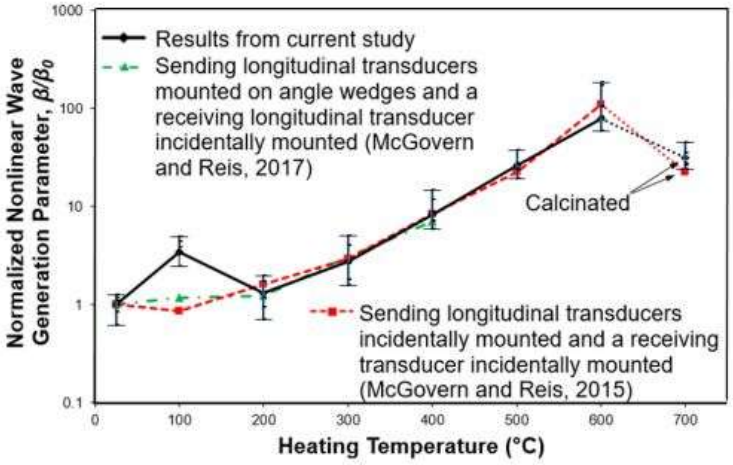

Figure 6.2: Normalized nonlinear wave generation parameter β/β0 as a function of heating temperature. The results of this diagram are reproduced from the work of Love, McGovern and Reis [7,14-16].

Note that in both cases, 100 °C specimen shows an irregularly high amplitude ratio comparing to that of specimen in 25 °C and 200 °C. This is because of the oil residue that remains in the

specimen. During the cutting process, mineral oil was used as the saw lubricant, and 100 °C is not sufficiently high enough vaporize the oil, thus leaving the oil in the specimen. Since the microcracks were filled with oil, it can greatly affect the nonlinear wave behavior. For 700 °C specimen, calcination process has made the amplitude ratio drop drastically. For detail about calcination, please refer to [27,28].

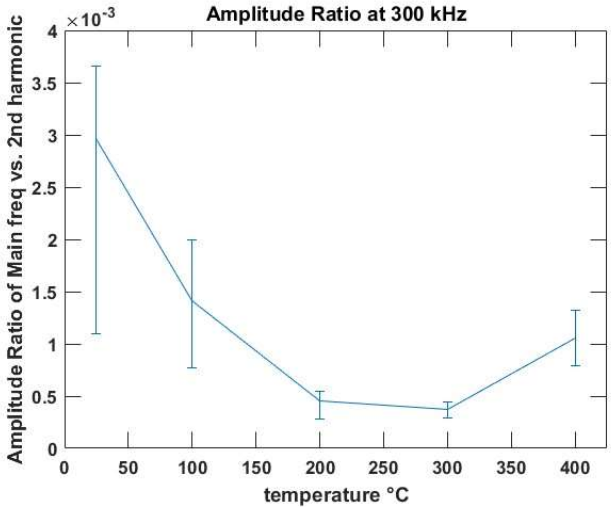

Figure 6.3: 2nd order amplitude ratio at 300 kHz. Note that specimens higher than 500 °C are not shown, as well as the third and fifth amplitude ratio.

At 300 kHz, the trend was partially represented from 25 °C to 400 °C specimens as shown in Figure 6.3. For 500 °C, 600 °C and 700 °C specimens, signals that at 500 kHz and above are transmitting at a significantly low amplitude as shown in Figure 6.4. Such inability to transmit high frequency signal was also shown in the linear characterization that is conducted by McGovern and Reis [14] as the velocity and attenuation of 500 °C, 600 °C and 700 °C specimens were unattainable. Reasons include destructive defects that causing the signal failed to transmit through the specimen and large attenuation caused by increasing microcracks making the wave scatters more. Note that at higher frequencies, high attenuation become major source of error as the trend of amplitude ratio at 300 kHz is greatly deviated from that at 100 kHz.

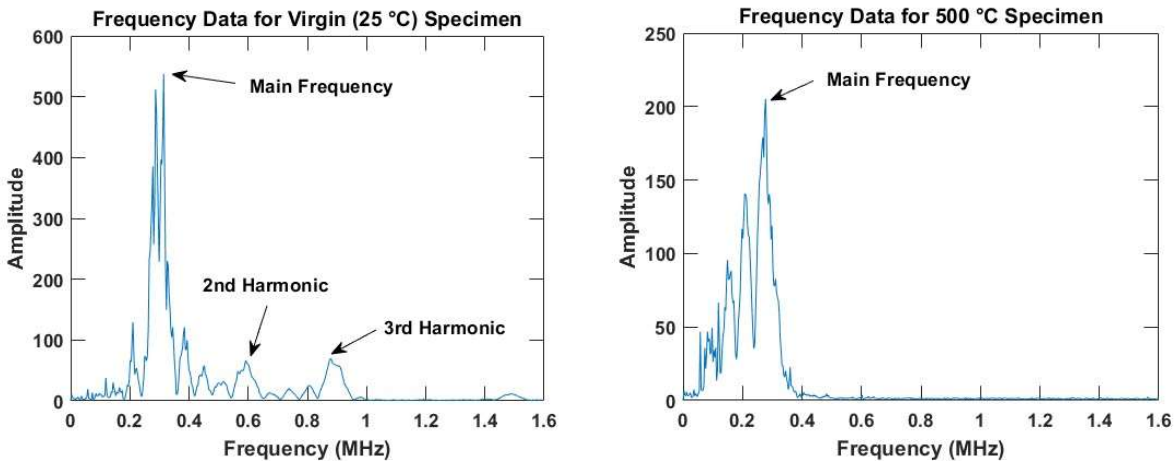

Figure 6.4: Frequency domain signal for Virgin specimen (left) and 500 °C specimen (right) when sending 300 kHz wave. Note that Virgin specimen has noticeable amplitude at higher harmonic frequencies, whereas 500 °C specimen has no noticeable component beyond main frequency mainly due to the higher attenuation.

The relationship between the flexural strength and amplitude ratio is shown in Figure 6.5. Data points for 25 °C specimen and 100 °C specimen are removed from this chart due to the deviation to expected value as reasoned above from the mechanism discussed in chapter 2. For both 3rd and 5th order amplitude ratio shows a strong correlation to Flexural Strength. Note that correlation equations here use logarithmic fit.

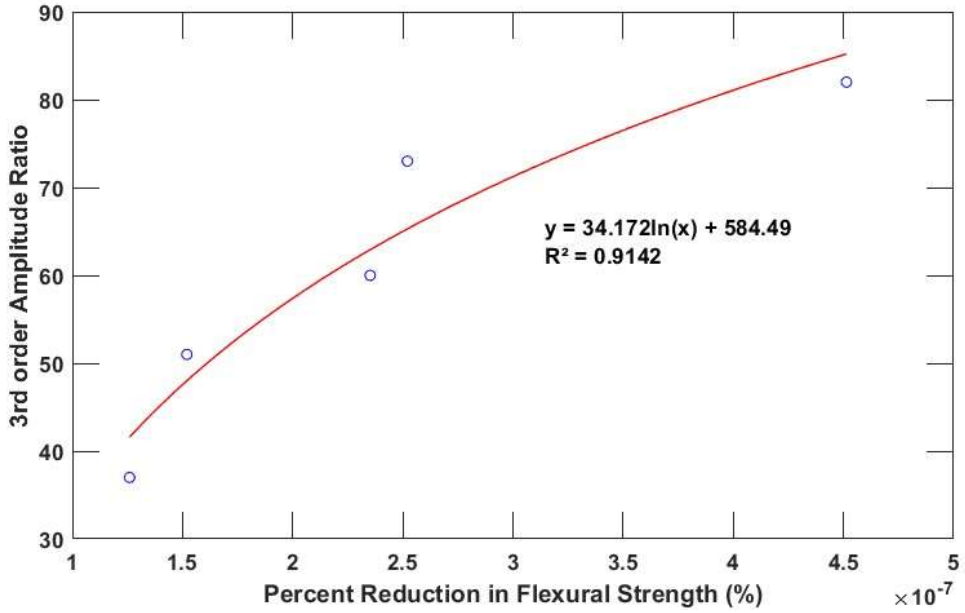

Figure 6.5 (cont.)

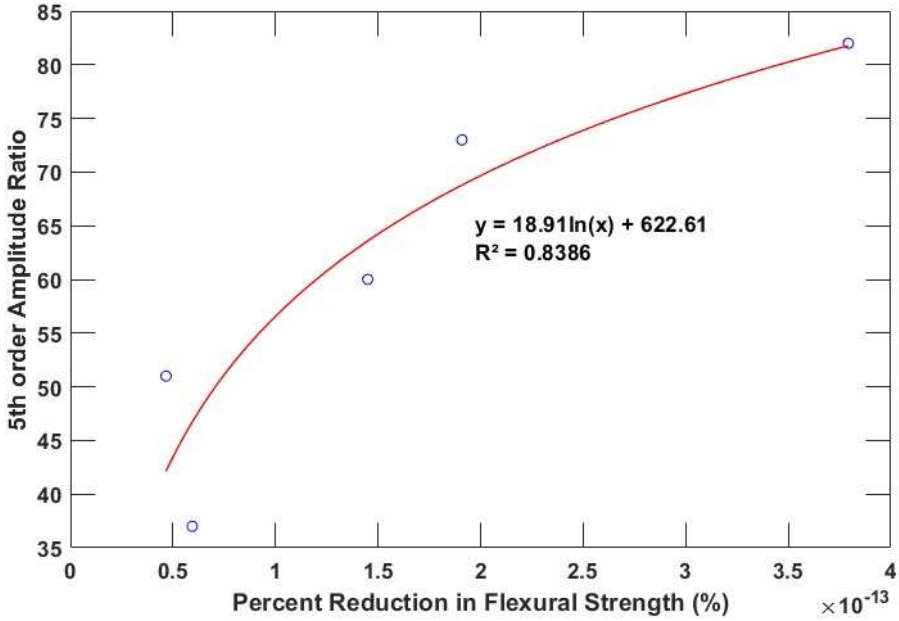

Figure 6.5: Percent reduction in flexural strength (with respect to the mean strength of the control sample) vs. the 3rd (up) and 5th (down) order of Amplitude Ratio. A Logarithmic fit is applied to the data without considering the 25 °C and 100 °C sample, as it is believed damage was not uniform in the sample (R^2 = 0.9141/0.8386). The data point corresponding to the 700 °C specimen is not included because of the material's calcination transformation.

CHAPTER 7: CONCLUSIONS AND FINAL RECOMMENDATIONS

7.1 Conclusion from test results

Dolomitic limestone specimens were heat treated to 25 °C, 100 °C, 200 °C, 300 °C, 400 °C, 500 °C, 600 °C and 700 °C and their corresponding flexural strength reductions were determined. Two longitudinal transducers were attached to the specimen as a through-transmission setup to send wave signal across the specimen and generate nonlinear higher harmonic behavior. It was found from the experiment that there is a positive correlation between the flexural strength reduction and amplitude ratio defined as the ratio between the amplitude at n-th harmonic frequency to the n-th power of amplitude at main frequency [17]. These two parameters have correlation factors of 0.9141 at 3^{rd} order ratio and 0.8386 at 5^{th} order ratio, proving that the generation of higher harmonic behavior is strongly correlated to the damage level, at least for heat treatment damage, of dolomitic limestone. Such finding validates the similar finding that were shown in studies of Love, McGovern and Reis [7,14-16] over a similar parameter. The experiment also distinguished that different order of amplitude ratio is sensitive to different physical parameters, as the increasing trend of 3^{rd} and 5^{th} order ratio behaved different at temperature range that higher harmonic method is most reliable. This finding can be further investigated along with the study conducted by Shah and Ribakov [17].

7.2 Recommendations for future work

Although this study has provided compelling evidence to establish the correlation between flexural strength reduction and the generation of nonlinear higher harmonic behavior, there are some considerable factors that may contribute to the error of this experiment.

First, equipment limitation causes the experiment to be conducted at a signal voltage that may not be high enough to excite higher harmonic component to expected level. For some specimens that have large attenuation at higher frequencies, signal voltage that is large enough will be beneficial for the experiment as the harmonic behavior may be excited.

Second, the signal mode should be excited at symmetric mode in order to receive even order harmonic signal component. It is ideal to investigate all harmonics' amplitude ratio so that the relationship between the ratios and physical properties of the material can be fully revealed. As shown in tests conducted at 100 kHz, no even harmonic frequencies have significantly high amplitude. This is preventable by changing the phase of sending signal.

Overall, the application of nonlinear higher harmonic generation can be a good tool to identify diffuse damage over material as it depends on material's inherent nonlinearities. However, it is premature to say that this technique is applicable to all materials as various factors may greatly affect the harmonic generation process. It is more reliable that this technique is cross referenced with other techniques such as velocity measurement, appearance judgement and acoustic emission. Also, tests conducting harmonic generation should be carefully calibrated so that no other source may affect the test results.

REFERENCES

1. Kuzvart, M., “Industrial Minerals and Rocks”, Elsevier, New York, (1984).
2. Freas, R.C., J.S. Hayden, and C.A. Pryor Jr., “Limestone and Dolomite,” Industrial Minerals and Rocks: Commodities, Markets, and Uses, Seventh Ed., Eds. J.E. Kogel, N.C. Trivedi, J.M. Barker and S.T. Krukowski, Colorado: Society for Mining, Metallurgy, and Exploration, Inc., pp. 581-597, (2006).
3. Boggs Jr., S. “Principles of Sedimentology and Stratigraphy”. 4th Edition, Pearson Education Inc., Upper Saddle River. pp. 172-187, (2006)
4. Kranjc, A. (2006). Baltazar Hacquet (1739/40-1815), “the Pioneer of Karst Geomorphologists.” Acta Carsologica, 35(2-3).
5. Fletcher, B., “A History of Architecture”, University of London, Athone Press, pp. 213-219, (1975).
6. Ashurst, J., and F.G. Dimes, Eds., “Conservation of Building and Decorative Stone”, 2000, Volume 1, p. 19, John Butterworth-Heinemann, London, England, p. 19, (2000).
7. Love, J. E. (2019). “Damage evaluation in dimension limestone using nonlinear ultrasonics.”, Master of Science thesis, University of Illinois at Urbana-Champaign, (2019).
8. Chin, I.R., “Common Causes of Failures of Stone Claddings on Buildings,” in “Dimension Stone Cladding: Design, Construction, Evaluation, and Repair,” ASTM STP 1394, K. R. Hoigard, Ed., American Society for Testing and Materials, West Conshohocken, PA, pp. 151-160, (2000).
9. Naggatz, S.G., and E.A. Gerns, “Full-Scale Flexural Strength Testing for Stone Cladding Design,” in “Dimension Stone Cladding: Design, Construction, Evaluation, and Repair,” ASTM STP 1499, K.R. Hoigard, and M.J. Scheffler, Eds., American Society for Testing and Materials, West Conshohocken, PA, pp. 3-10, (2007).
10. ASTM Standard C 880-06, “Standard Test Method for Flexure Strength of Dimension Stone,” Annual Book of Standards, Vol. 4.07, ASTM International, West Conshohocken, PA, (2007).
11. ASTM Standard C 170, “Standard Test Method for Compressive Strength in Natural Building Stone,” Annual Book of Standards, Vol. 15.06, ASTM International, West Conshohocken, PA, (2001).

12. ASTM Standard C 99, “Standard Test Method for Modulus of Rupture in Natural Building Stone,” Annual Book of Standards, Vol. 15.06, ASTM International, West Conshohocken, PA, (2001).
13. Schouenborg, B., B. Grelk, and K. Malage, “Testing and Assessment of Marble and Limestone (TEAM)—Important Results from a Large European research Project on Cladding Panels,” in “Dimension Stone Cladding: Design, Construction, Evaluation, and Repair,” ASTM STP 1499, K.R. Hoigard, and M.J. Scheffler, Eds., American Society for Testing and Materials, West Conshohocken, PA, pp. 124-137, (2007).
14. Megan E, Govern Mc, Reis H (2015) “Damage characterization in dimension limestone cladding using non- collinear ultrasonic wave mixing.” Optical Engineering, 55(1): 011012-12.
15. Megan E, Govern Mc, Reis H (2014) “Linear and nonlinear characterization of limestone rock using a non- collinear ultrasonic wave mixing.” Proceedings of SPIE 9064, Health Monitoring of Structural and Biological Systems, 906404.
16. Megan E, Govern Mc, Reis H (2017) “Nonlinear ultrasonic damage characterization in limestone.” Research in Nondestructive Evaluation 28(4): 226-240.
17. A.A. Shah, Y. Ribakov (2009) “Non-linear ultrasonic evaluation of damaged concrete based on higher order harmonic generation.” Materials and Design 30 (2009) 4095–4102
18. Siegesmund, S., Ullemeyer, Weiss, K.T., and Tschegg, E.K., (2000), “Physical weathering of marbles caused by anisotropic thermal expansion,” International Journal of Earth Science, 89:170-182.
19. “Tower of London from the Shard”, Wikimedia, https://commons.wikimedia.org/wiki/File:Tower_of_London_from_the_Shard_(8515883950).jpg
20. “Tower of London”, World Heritage Convention, https://whc.unesco.org/en/list/488/
21. Carlos, A., I. Masumi, M. Hiroaki, M. Maki, and O. Takahisa, “The effects of limestone aggregate on concrete properties,” Construction and Building Materials, 24(12), 2363-2368 (2010).
22. Sybilski, D., W. Bańkowski, and M. Krajewski, “High Modulus Asphalt Concrete with Limestone Aggregate,” International Journal of Pavement Research and Technology, 3(2) 96-101 (2010).

23. Clancy, T.A.; Benson, D.J. (2009). "Refractory Dolomite Raw Materials". Raw Materials for Refractories Conference. Vol. 38. John Wiley & Sons. p. 119.
24. Miglio, B.F., D.M. Richardson, T.S. Yates, and D. West, "Assessment of the Durability of Porous Limestones: Specification and Interpretation of Test Data in UK Practice," Dimension Stone Cladding: Design, Construction, Evaluation, and Repair, ASTM STP 1394, K.R. Hoigard, Ed., ASTM, W. Conshohocken, Pennsylvania, (2000).
25. Logan, J. M., "Laboratory and case studies of thermal cycling and stored strain on the stability of selected marbles," Environ. Geol. 46: 456-467 (2004).
26. Royer-Carfagni, G., "Some considerations on the warping of marble facades: the example of Alvar Aalto's Finland Hall in Helsinki," Constr. Build. Mater. 13: 449-457 (1999).
27. Kumar, G. S., A. Ramakrishnan, and Y.-T. Hung, "Lime calcination in Advanced Physicochemical Treatment Technologies Handbook of Environmental Engineering," L. K. Wank, Y.-T. Hung, and N. K. Shammas, Eds., 5:611-633, Humana Press, New Jersey (2007).
28. Britton, H. T. S., S. J. Gregg, and G. W. Winsor, "The calcination of dolomite: part II. The thermal decomposition of dolomite," Trans. Faraday Soc. 48: 70-75 (1952).
29. Collie, Robert L. "Solar heating system" U.S. Patent 3,955,554 issued May 11, 1976
30. Selleck SF, Landis EN, Peterson ML, Shah SP, Achenbach JG. "Ultrasonic investigation of concrete with distributed damage." ACI Mater J 1998;95(1):27–36.
31. Suaris W, Fernando V. "Ultrasonic pulse attenuation as a measure of damage growth during cyclic loading of concrete." ACI Mater J 1987;84(3):185–93.
32. Hurley DC, Fortunko CM. "Determination of the non-linear ultrasonic parameter using Michelson interferometer." Meas Sci Technol 1997;8:634–42
33. Zheng Y, Maev RG, Solodov IY. "Non-linear acoustic applications for material characterization: a review." Can J Phys 1999;77:927–67.
34. Guyer, R.A., and P.A. Johnson, "Nonlinear Mesoscopic Elasticity: Evidence for a New Class of Materials," American Institute of Physics, Physics Today, 52(4):30-36 (1999).
35. Guyer, R.A., and P.A. Johnson, "Nonlinear Mesoscopic Elasticity: The Complex Behavior of Granular Media Including Rocks and Soil," Weinheim: Wiley, (2009).
36. Kim J, Jacobs J, Qu J, Littles, JW (2006) "Experimental characterization of fatigue damage in nickel- base super alloy using nonlinear ultrasonic waves." J of Acous. Society of America, 120: 1266-1273.

37. Maev RG, Solodov IY. “Acoustic reflectivity enhancement using higher-order non-reflection mode.” IEEE Ultrason Sympos 1998:707–10.
38. Cantrell JH. “Fundamentals and applications of non-linear ultrasonic nondestructive evaluation.” In: Kundu Tribikram, editor. Ultrasonic non-destructive evaluation, vol. 6. Boca Raton (FL): CRC Press; 2004. p. 363– 434
39. Shah AA, Ribakov Y, Hirose S. “Non-destructive evaluation of damaged concrete using non-linear ultrasonics.” Mater Des 2009;30(3):775–82.
40. “Dolomitic Limestone”, Wikimedia, https://commons.wikimedia.org/wiki/File:Dolomitic_Limestone.JPG
41. “Ohio Statehouse 03”, Wikimedia, https://commons.wikimedia.org/wiki/File:Ohio_Statehouse_03.jpg
42. “Romania-1170 - Palace of the Parliament”, Wikimedia, https://commons.wikimedia.org/wiki/File:Romania-1170_-_Palace_of_the_Parliament_(7557749966).jpg
43. Len KS, Solodov IY. “Non-linear reflection of surface waves at a contact interface between solids.” Acoust Phys (USA) 1993;39:149–51.
44. Na JK, Breazeale M. “Ultrasonic non-linear properties of lead zirconate–titanate ceramics.” J Acoust Soc Am JASA 1994;95:3213–21.
45. C. J. Lissenden, Y. Liu, G. W. Choi, X. Yao, “Effect of Localized Microstructure Evolution on Higher Harmonic Generation of Guided Waves”, J Nondestruct Eval (2014) 33:178–186
46. Ankit Srivastava, Francesco Lanza di Scalea, “On the existence of antisymmetric or symmetric Lamb waves at nonlinear higher harmonics”, Journal of Sound and Vibration, Volume 323, Issues 3–5, 2009, 932-943
47. Sassoni, E., Naidu, S., and Scherer, G.W., 2011, “The use of hydroxyapatite as a new inorganic consolidant for damaged carbonated stones,” Journal of Culture Heritage, Vol. 12, pp. 346-355.
48. Franzoni, E., Sassoni, E., Scherer W., George, and Naidu, S., 2013, “Artificial weathering of stone by heating,” Journal of Culture Heritage, vol. 14S, pp. e85-e93.
49. Kim, J.Y., Treiber, M., and Jacobs, L.J., (2009), “A Switching Technique for Measuring High Ultrasonic Attenuation,” Rev. of Quantitative Nondestructive Evaluation, American Inst. of Physics, Vol. 28, pp. 1611-1618.

APPENDIX A: SWITCHING TECHNIQUE FOR ATTENUATION MEASUREMENTS

Attenuation measurement is a part of the linear characterization that was used to determine the amplitude ratio. From equation (19), theoretically, attenuation coefficient can be directly determined the same through-transmission data studying amplitude ratio as shown:

$$A_1 = A_2 \exp(-\alpha d) \tag{21}$$

Here, A_1 and A_2 are the amplitudes of the received and rebound tunebursts as indicated in Figure A.2, α is attenuation coefficient and d is the traveling distance for rebound bursts, which is twice the width of the measuring specimen. However, this measuring method is not fully correct as it does not account loss between the transducer and specimen.

In order to correctly measure the attenuation, a switching technique [49] is used in this study. As illustrated in the schematic diagram in Figure A.1, a set of 5 independent tests are needed for this technique and 6 amplitudes will be collected. Assume sending wave has an amplitude of A_0, each amplitude can be calculated through following equations:

$$A_1 = A_0 T_{1s} T_{s1} R_R \exp(-2\alpha d) \tag{22}$$

$$A_2 = A_0 T_{1s} T_{s1} R_{RT} \exp(-2\alpha d) \tag{23}$$

$$A_3 = A_0 T_{1s} T_{s2} \exp(-\alpha d) \tag{24}$$

$$A_4 = A_0 T_{2s} T_{s2} R_{LT} \exp(-2\alpha d) \tag{25}$$

$$A_5 = A_0 T_{2s} T_{s2} R_L \exp(-2\alpha d) \tag{26}$$

$$A_6 = A_0 T_{1s} T_{s2} R_{RT} R_{LT} \exp(-3\alpha d) \tag{27}$$

Here, T_{1s}, T_{s1}, T_{2s} and T_{s2} are the transmission coefficients of a) from transducer 1 to specimen, b) from specimen to transducer 1, c) from transducer 2 to specimen and d) from specimen to transducer 2. R_R, R_{RT}, R_L and R_{LT} are the reflection coefficients of surfaces that a) has no transducer on the right side, b) has transducer on the right side, c) has no transducer on the left side and d) has transducer on the left side. In general cases, R_R and R_L are considered as 1 since the impedance of specimen is considerably larger than that of air. A mathematical relationship between A_3 and A_6 can be conducted as:

$$\frac{A_6}{A_3} = R_{RT}R_{LT}\exp(-2\alpha d) = \frac{A_2}{A_1}\cdot\frac{A_4}{A_5}\exp(-2\alpha d) \tag{28}$$

$$\alpha = -\frac{\ln\left(\frac{A_1A_5A_6}{A_2A_3A_4}\right)}{2d} \tag{29}$$

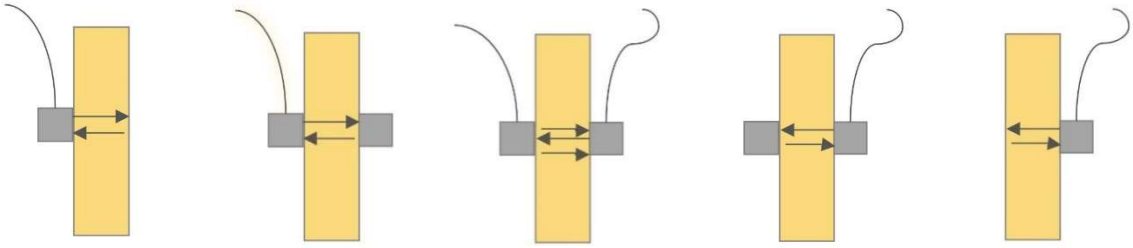

Figure A.1: A standard set of switching technique attenuation measurement tests: a) only transducer 1 is attached and connected, first reflected signal's maximum amplitude is collected as A_1; b) transducer 1 and 2 are attached, only transducer 1 is connected, first reflected signal's maximum amplitude is collected as A_2; c) transducer 1 and 2 are attached and connected, through transmitted signal and first rebound signal's maximum amplitudes are collected as A_3 and A_6; d) transducer 1 and 2 are attached, only transducer 2 is connected, first reflected signal's maximum amplitude is collected as A_4; e) only transducer 2 is attached and connected, first reflected signal's maximum amplitude is collected as A_5.

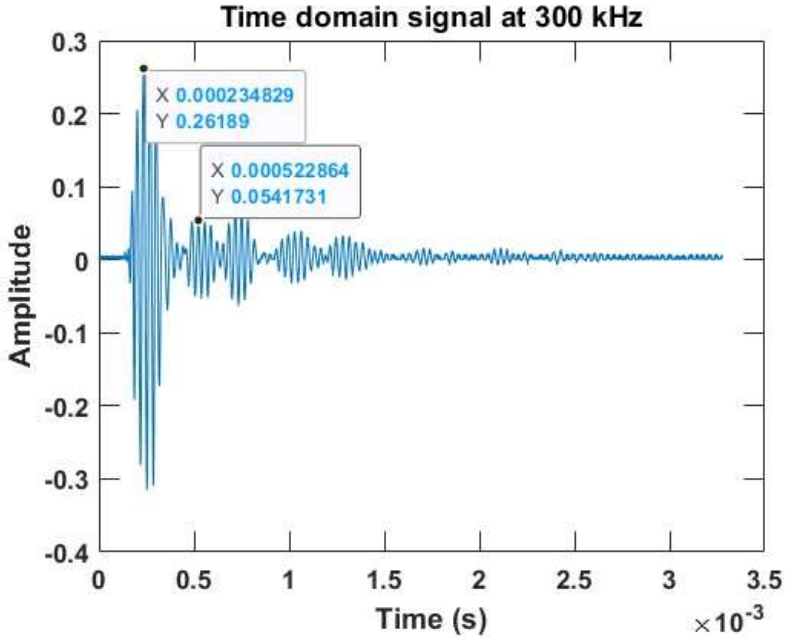

Figure A.2: Time domain signal of test (c) for virgin specimen at 300 kHz with amplitude and time data points of the receiving bang (left) and first reflection bang (right). Data points that are highlighted in the graph will be collected as A_3 and A_6.

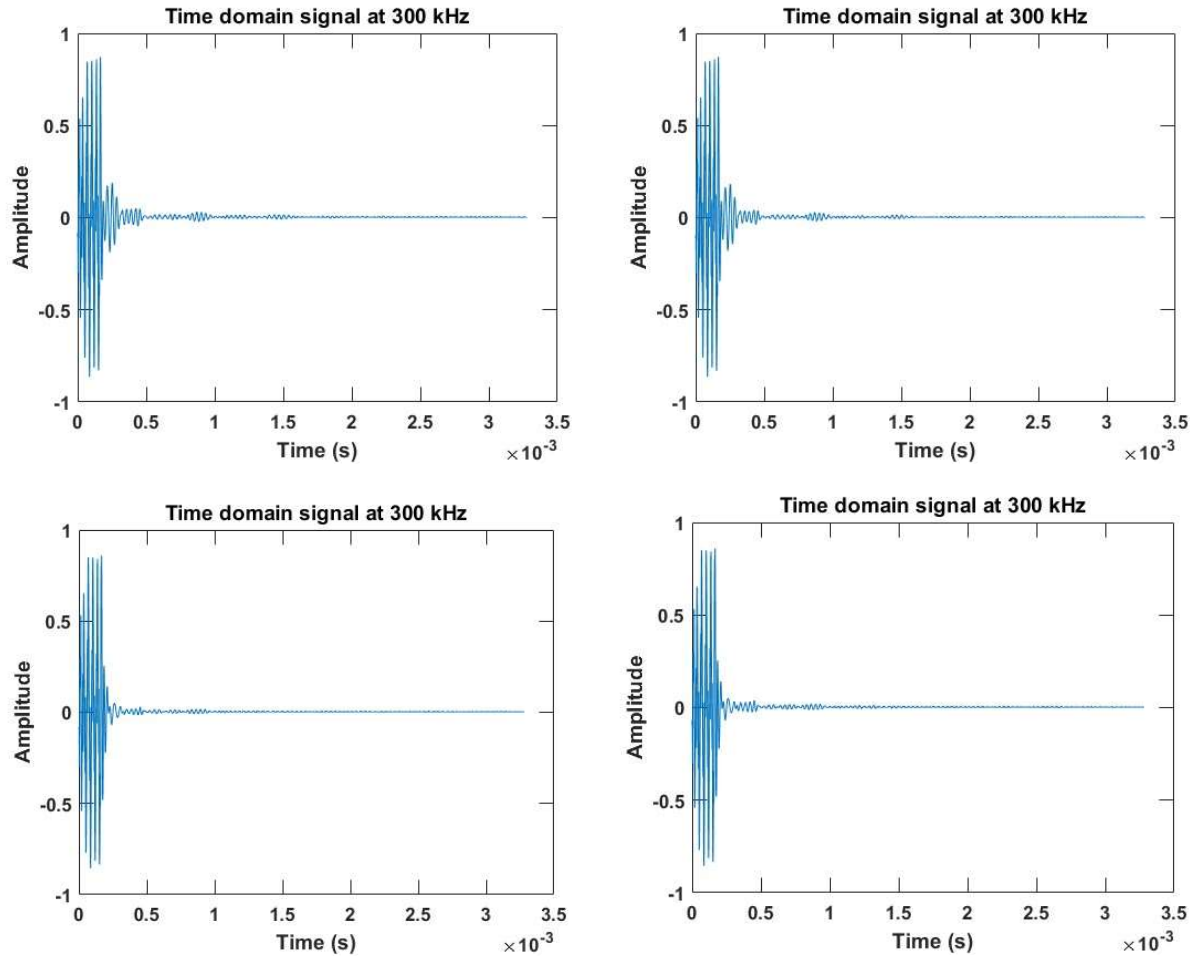

Figure A.3: Time domain signals of test (a), (b), (d), (e) for virgin specimen at 300 kHz.